Direct and indirect roles of CNS dorsal midline cells in choroid plexus epithelia formation

D. Spencer Currle, Xun Cheng, Ching-mei Hsu and Edwin S. Monuki*

Departments of Pathology and Developmental and Cell Biology, University of California, Irvine, D440 Medical Sciences I, Irvine, CA 92697-4800, USA

*Author for correspondence (e-mail: emonuki@uci.edu)

Accepted 23 May 2005

Development 132, 3549-3559
Published by The Company of Biologists 2005
doi:10.1242/dev.01915

Summary

Choroid plexus (CP) produces the cerebrospinal fluid (CSF) of the central nervous system (CNS), but little is known about the mechanisms underlying development of this important tissue. CP forms in the hindbrain (4th ventricle), diencephalon (3rd ventricle) and dorsomedial telencephalon bilaterally (lateral ventricles). All of these sites lie at or near the embryonic dorsal midline (DM), which acts as a CNS patterning center. We therefore examined DM-CP relationships using normal and Gdf7 (Bmp12) transgenic embryos to fate map or ablate DM cells. These studies revealed a Gdf7 fate map that includes most CP epithelial (CPe) cells of the hindbrain and diencephalon. In the telencephalon, Gdf7 cell lineages were found in the small anterior domain of telencephalic CPe (tCPe), but its large posterior domain was devoid of these lineages. Anterior and posterior tCPe domains, which arise within a contiguous field separate from diencephalic CPe, also exhibited different patterns of apoptosis. Despite lacking Gdf7 cell lineages, the posterior tCPe domain failed to form after ablating Gdf7-expressing DM cells at neural tube stages. The tCPe loss was associated with abrogation of high-level bone morphogenetic protein (Bmp) signaling, which is known to be required for tCPe induction. Taken together, these studies demonstrate intimate DM-CPe relationships throughout the CNS and highlight two distinct tCPe domains, including a posterior domain whose genesis depends on DM cells in a non-cell-autonomous fashion.

Key words: Roof plate, Fate map, Genetic ablation, Bmp, Gdf7, Transgenic mice, Cre recombinase, Diphtheria toxin, Mouse

Introduction

The choroid plexus (CP) produces the cerebrospinal fluid (CSF) that surrounds the brain and spinal cord, and fills the ventricular system. The CP and CSF are thought to have multiple functions (e.g. nutritive, mechanical, metabolic, neuroendocrine, immune) in brain physiology and neurological diseases. The CP also serves as an important point of entry for therapeutic drugs, as it is a major component of the blood-CSF and blood-brain barriers. Defects in CSF flow, resorption or production lead to hydrocephalus, a common developmental disorder with an estimated incidence of 1 per 500 live births. Furthermore, the CP has been implicated as a secondary signaling center during early CNS development (Yamamoto et al., 1996). Despite this significance, relatively little is known about the mechanisms underlying CP development.

CP forms in three locations at or near the dorsal midline of the central nervous system (CNS) – in the hindbrain roof (myelencephalic CP of the 4th ventricle), in the anterior diencephalic roof (diencephalic CP of the 3rd ventricle), and at the dorsomedial edges of the telencephalon bilaterally (telencephalic CP of the lateral ventricles) (Fig. 1A). CP contains both epithelial and mesenchymal (stromal) components, with the CP epithelium (CPe) facing the ventricular lumen. CPe is a single-layered cuboidal to columnar epithelium that is contiguous with adjacent pseudostratified neuroepithelium. At all sites of CPe formation in mice, differentiation into a simple epithelium occurs by embryonic day 12.5 (E12.5) (Sturrock, 1979) and is accompanied by activation of the CPe-specific gene transthyretin (*Ttr*) (Harms et al., 1991; Herbert et al., 1986). Interactions between the epithelium and mesenchyme (Wilting and Christ, 1989) are then thought to transform the CP into a true vascular plexus with its hallmark papillary architecture.

The embryonic dorsal midline (DM) is a well known CNS patterning center (Chizhikov and Millen, 2005; Furuta et al., 1997; Lee et al., 2000a; Liem et al., 1997; Millonig et al., 2000; Monuki et al., 2001) that is ideally positioned to regulate CP development (Fig. 1A). The DM includes the roof plate (RP), the midline 'roof' of the neural tube that forms when the neural plate fuses. In mice, neural plate fusion begins in the occipital/cervical region at E8.0-8.5, then proceeds rostrally and caudally, with fusion in the forebrain occurring during the E8.5-9.0 period (Kaufman and Bard, 1999). The RP specifies and patterns dorsal neural tissues via signaling proteins, most notably the bone morphogenetic proteins (Bmps) (Furuta et al., 1997; Lee et al., 2000a; Liem et al., 1997). In the telencephalon, the RP is closely associated with the telencephalic CPe (tCPe) and cortical hem (Fig. 1B), where both Bmps and Wnts are expressed (Grove et al., 1998; Lee et al., 2000b). Owing to imprecision in defining the spatiotemporal boundaries between the RP, tCPe and hem, we refer to this region collectively as the 'DM' at neural tube

stages (E9.5-10.5). At later stages, when hem and tCPe differentiation are apparent (e.g. E11.5-12.5), we refer to this region as the 'dorsomedial telencephalon' (DMT) (Fig. 1B).

Despite the likelihood of important DM-CP relationships, remarkably little evidence for such relationships exist. Genetic fate mapping has suggested lineage relationships between DM and CPe cells in the hindbrain (Awatramani et al., 2003). In the telencephalon, inactivations of the BmpRIa receptor indicated a requirement for local high-level Bmp signaling in tCPe induction (Hebert et al., 2002). We have previously reported studies with two Gdf7 transgenic mouse lines – Gdf7Cre and Gdf7DTA (Lee et al., 2000a) – that allowed for selective fate mapping or ablation of Gdf7-expressing DM cells (Monuki et al., 2001). Gdf7-mediated ablations resulted in CPe loss, but the CPe phenotype was confounded by an open neural tube defect that involved the forebrain (Monuki et al., 2001). In this study, we used two Gdf7-mediated ablation strategies that correct the open forebrain defect, together with detailed genetic fate mapping and apoptosis studies, to demonstrate intimate DM-CPe relationships at all sites of CP formation.

Materials and methods

Mice

For timed pregnancies, noon of the vaginal plug date was day 0.5; developmental stage was confirmed by embryo crown-rump measurement. The following mice were used: Gdf7Cre (Lee et al., 2000a) with *rosa26* conditional *lacZ* reporter [R26R, 129S-Gt(ROSA)26Sor$^{tm1Sor/J}$; Jackson Laboratories] (Soriano, 1999) for Gdf7 fate mapping; Gdf7Cre with Gdf7-XstopX-DTA (Gdf7DTA) (Lee et al., 2000a) for late ablation; βactin-Cre [ACTBCre, FVB/N-TgN(ACTB-Cre)2Mrt; Jackson Laboratories] (Lewandoski et al., 1997) with Gdf7DTA for early ablation; ACTBCre with R26R for control studies; CD1 or C57BL/6 (Charles River) for wild-type studies. Genotypes were determined by gross morphology (ACTBCre;Gdf7DTA) and PCR genotyping of tail DNA for Cre, DTA and/or neo (Monuki et al., 2001). Mutant embryos with open forebrain defects were excluded from analysis. All animal studies were carried out according to institutional IACUC guidelines.

X-gal histochemistry, in situ hybridization, histology and TUNEL assays

These were performed as described (Monuki et al., 2001) with the following modifications: (1) for X-gal staining, embryos were fixed at 4°C in either 4% paraformaldehyde (1-2 hours) or 0.2-0.4% paraformaldehyde (4 hours to overnight) supplemented with 2 mM $MgCl_2$ and 5 mM EGTA; (2) for section in situ hybridization, Proteinase K digestion was omitted, and coverslips were elevated using PCR sealing tape to reduce edge artifact and minimize tissue disruption. Paraffin sections were processed and sectioned by the UCI Pathology Services Core. The following in situ hybridization probe templates were used: mouse Ttr EST (IMAGE clone 1078224, Accession Number AA822938), mouse Gdf7 cDNA (from Candice Crocker and Anne Calof), mouse Bmp4, Bmp6 and Bmp7 cDNAs (from Julie Lauterborn) (Furuta et al., 1997), and mouse Msx1 EST (IMAGE clone 903377, Accession Number AA518368). Fluorescent TUNEL was performed according to manufacturer protocol (Apoptag kit, Serologicals) with Hoechst 33342 (Molecular Probes) nuclear counterstaining on 10-20 μm cryosections. Images were captured by Spot RT digital imaging on a Nikon SMZ1500 stereodissecting microscope or upright Nikon E600 microscope with bright-field, DIC or fluorescence optics. For comparative studies (mutant versus littermate controls, serial section analysis), processing steps and assays were carried out in parallel, and images were captured using identical camera settings and image enhancements. In the few cases where littermate control sections were unavailable, wild-type sections were used.

qRT-PCR

Real-time semi-quantitative RT-PCR was established using rigorous quality controls (Stankovic and Corfas, 2003) to validate all assumptions embedded in the standard ΔΔCt method for quantifying relative expression levels (Livak and Schmittgen, 2001). Mouse 18S (Stankovic and Corfas, 2003), cyclophilin A and intron-spanning Ttr primers from PrimerBank (Wang and Seed, 2003) were commercially prepared (Qiagen) and verified for amplification efficiency and constancy over four to six logs of template concentration on an Opticon System (MJ Research) using SYBR-Green-containing master mixes (MJ Research/Biorad). Amplicon sizes were verified by gel electrophoresis; the Ttr amplicon was also confirmed by sequencing. Among four internal references tested (18S, CYPA, GAPDH, actin), 18S and CYPA varied the least between E12.5 ACTBCre;Gdf7DTA mutants and littermate controls. Total dorsal forebrain RNA was column purified (Aurum mini kit, Biorad), then reverse transcribed with MMLV RT (Promega) and random primers. 18S QPCR was performed on all corresponding cDNA and RNA samples; all $\Delta Ct_{cDNA\text{-}RNA}$ are at least 16.7 (mean 20.9), which indicates a cDNA:genomic target ratio of more than 10^5. Ttr measurements in three E12.5 ACTBCre;Gdf7DTA mutant and three control littermate samples were performed in duplicate in a single experimental run. One obvious outlier Ct value was discarded; all other samples were well duplicated ($\Delta Ct<0.5$). Duplicate Ct, normalized ΔCt ($Ct_{Ttr} - Ct_{reference}$), ΔΔCt ($\Delta Ct_{mutant}$ – average $\Delta Ct_{control}$), and relative level ($2^{-\Delta\Delta Ct}$) means and s.e.m. were calculated in Excel and graphed in KaleidaGraph.

Results

Gdf7 activation is restricted to DM neuroepithelium at neural tube stages

We first performed Gdf7Cre × R26R matings to study the Gdf7 fate map in detail (Fig. 1C). Gdf7Cre;R26R double transgenic embryos from this cross display permanent *lacZ* expression in Gdf7 cell lineages – i.e. in cells that initially activate Gdf7 as well as their descendants. No *lacZ* expression was detected in E8.5 embryos (data not shown). By E9.5, labeling became detectable in a DM-restricted pattern throughout the CNS, including the hindbrain, diencephalon and telencephalon (Fig. 2A,B). Gdf7 activation occurred slightly earlier in the diencephalon and hindbrain compared with the telencephalon, where labeling was detectable only in larger, more developmentally advanced E9.5 littermates.

By E10.5, X-gal staining became stronger and remained confined to the DM (Fig. 2C-G). In the telencephalon, the labeled DM domain was broader than that in the diencephalon, and these two domains were separated by weaker staining at the midline between the telencephalon and diencephalon (the di-telencephalic midline boundary; Fig. 2C). Sections through the telencephalon demonstrated primary localization of labeled cells to DM neuroepithelium, including the RP. Many, but not all telencephalic DM cells were labeled, and the intracellular labeling patterns were suggestive of recent *lacZ* expression onset (i.e. X-gal staining in perinuclear organelles rather than diffusely in the cytoplasm; Fig. 2E,G).

Few, if any, labeled cells were found away from the telencephalic DM anteriorly, laterally in the cortical primordia, or radially in overlying mesenchyme and epidermal ectoderm. Confinement to the DM was also relatively strict in the

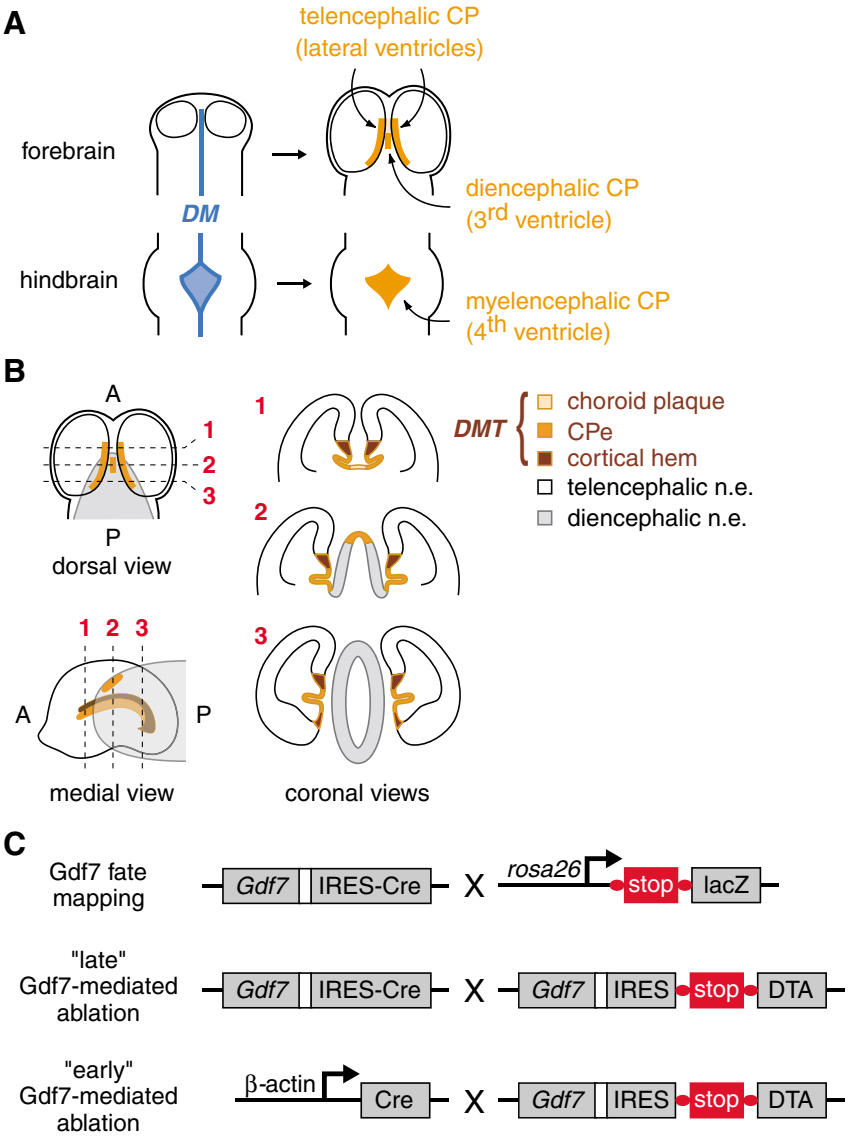

Fig. 1. (A) Dorsal schematics of the E9.5-10.5 neural tube (left) and E12.5 CNS (right); rostral is towards the top and caudal is towards the bottom. In the neural tube, the dorsal midline (DM, blue) of the hindbrain has a rhomboidal shape owing to unique morphogenetic movements (Alexandre and Wassef, 2003; Awatramani et al., 2003). Choroid plexus (CP, orange) forms at or near the midline in the hindbrain (4th ventricle), diencephalon (3rd ventricle) and dorsomedial telencephalon bilaterally (lateral ventricles). Whether the diencephalic and telencephalic CP are separate or continuous was uncertain. Ovals designate the telencephalon. (B) Schematics of dorsal and medial views of E12.5 forebrain, showing the positions of sections 1-3 on the right. The medial view, adapted from in situ hybridization images (Grove et al., 1998), illustrates one telencephalic hemisphere with overlying diencephalon (gray). The dorsomedial telencephalon (DMT) consists of telencephalic CP epithelium (CPe) and cortical hem (brown). At anterior DMT levels (section 1), these bilateral structures are separated by the choroid plaque and occupy a midline position. After reaching the diencephalon (section 2), the bilateral DMT are dorsomedial rather than midline and contiguous with both telencephalic and diencephalic neuroepithelium. Once past the interventricular foramina (section 3), the DMT loses its diencephalic connection and becomes contiguous solely with other telencephalic structures. (C) Schematics of the transgenic mating strategies used in this study; see text for details. A, anterior; CP, choroid plexus; CPe, choroid plexus epithelium; DM, dorsal midline; DMT, dorsomedial telencephalon; n.e., neuroepithelium; P, posterior.

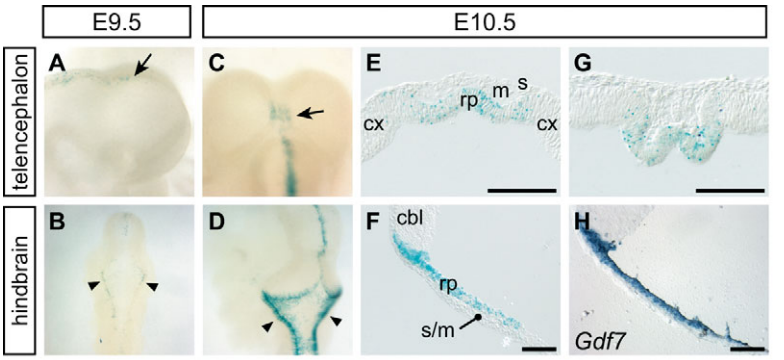

Fig. 2. Gdf7 activation in DM neuroepithelium at neural tube stages. X-gal stains of Gdf7Cre;R26R embryos (A-D) and coronal sections (E-G), and wild-type Gdf7 in situ hybridization (H); rostral is rightwards in A, towards the top in B-D. (A,B) E9.5 embryos. *lacZ* is weakly detected in the DM throughout the CNS, including the telencephalon (arrow in A) and hindbrain (arrowheads in B). (C,D) E10.5 embryos. *lacZ* is more readily detected in the DM of the telencephalon (arrow in C), diencephalon (C) and hindbrain (arrowheads in D). The telencephalic and diencephalic DM domains are separated by weaker staining at the di-telencephalic midline boundary (C). (E,G) E10.5 telencephalon. Labeling is detected in many, but not all, DM neuroepithelial cells in the roof plate (rp). Little to no labeling is seen laterally in the cortical primordia (cx) or radially in the overlying mesenchyme (m) and surface ectoderm (s). (F,H) E10.5 hindbrain. X-gal staining (F) and Gdf7 transcripts (H) are primarily localized to RP neuroepithelium and its junction with the cerebellar anlage (cbl), with little to no expression in surface ectoderm or overlying mesenchyme (s/m). Scale bars: 0.1 mm.

hindbrain, diencephalon and midbrain at E10.5 (Fig. 2C,D,F). The location of Gdf7 transcripts in wild-type E10.5 embryos, as detected by in situ hybridization, matched the genetic fate map well (Fig. 2H, see Fig. 10B). Thus, at neural tube stages (E9.5-10.5), Gdf7 activation is restricted to DM neuroepithelial cells throughout the developing CNS.

The Gdf7 fate map in the hindbrain and diencephalon includes mCPe and dCPe

We next studied Gdf7Cre;R26R embryos from E11.5-14.5, when definitive CPe differentiation occurs at all sites. Most of the myelencephalic and diencephalic CPe (mCPe and dCPe, respectively) showed strong *lacZ* expression, while CP mesenchyme was devoid of labeling (Fig. 3E,F,I-L). In addition to CPe cells, labeling in the hindbrain was strong at the junctions between mCPe and adjacent neuroepithelium (cerebellum rostrally, myelencephalon caudally; Fig. 3J,L). In the diencephalon, *lacZ* expression was detected further away from the midline in pseudostratified neuroepithelium (Fig. 3E,F). As seen at neural tube stages, localization of Gdf7 transcripts (Fig. 3A,B,G,H) matched the genetic fate map well, but also suggested ongoing Gdf7 transcription in mCPe and dCPe cells at E12.5, which prevents definitive evaluation of lineage (i.e. CPe cells derived from Gdf7-negative precursors could activate Gdf7 after becoming CPe). Nonetheless, these studies were suggestive of DM-to-CPe lineages in the mCPe and dCPe.

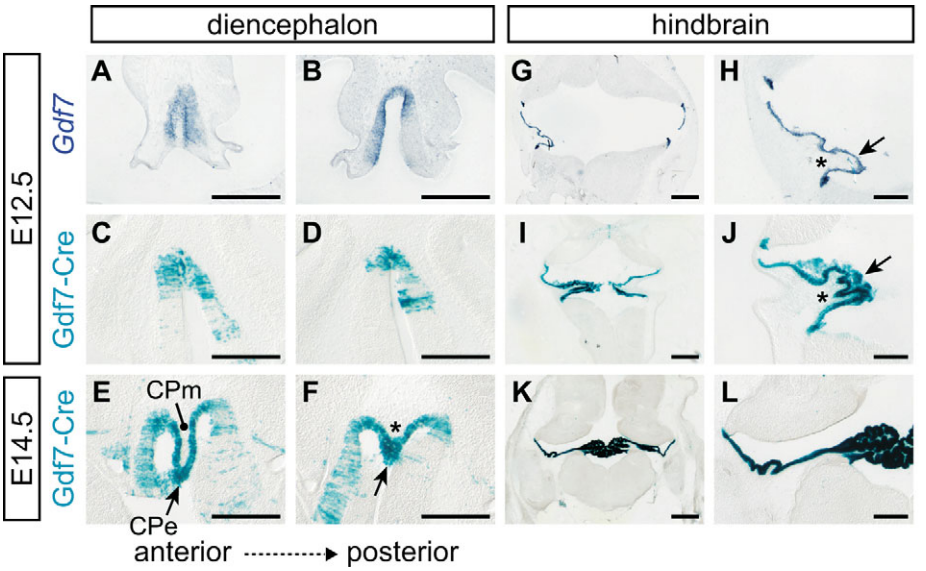

Fig. 3. Gdf7 fate mapping to the diencephalic and myelencephalic CPe. Gdf7 in situ hybridization (A-B,G-H) and X-gal staining (C-F,I-L) on wild-type or Gdf7Cre;R26R coronal cryosections. Sections in B,D,F are 40-60 μm posterior to those in A,C,E, respectively. (A-F) Diencephalon (3rd ventricle). Gdf7 transcripts mark the E12.5 diencephalic midline and adjacent neuroepithelium (A,B). The E12.5 Gdf7 fate map highlights the same regions as Gdf7 in situ hybridization (C,D), as well as the dCPe at E14.5 (E,F). (G-L) Hindbrain (4th ventricle). Gdf7 transcripts are detected in the mCPe (G,H), and most mCPe cells belong to the Gdf7 fate map (I-L). Prominent labeling is also seen at the junctions between mCPe and adjacent neuroepithelium (cerebellum rostrally, myelencephalon caudally), but little labeling is seen elsewhere at these stages. Scale bars: 0.4 mm in G,I,K; 0.2 mm in A-F,H,J,L.

The Gdf7 fate map in the telencephalon includes anterior, but not posterior, tCPe cells

In the E11.5 and E12.5 telencephalon, labeled cells in Gdf7Cre;R26R embryos were primarily located in the DMT, at levels rostral to the diencephalon (Fig. 4A,D). This anterior domain of the DMT consists of three structures: (1) the midline choroid plaque, (2) the bilateral tCPe and (3) the bilateral cortical hem (Fig. 1B). In contrast to the hindbrain and diencephalon (Fig. 3), the lack of detectable Gdf7 transcripts in the DMT or other telencephalic regions after E10.5 (Fig. 4G-I) suggested that the labeled anterior DMT cells were lineally related to the Gdf7-expressing DM cells at neural tube stages (Fig. 2C,E,G). Gdf7 cell lineages constituted a smaller fraction of the E11.5-12.5 anterior DMT compared with the E9.5-10.5 DM, and this fraction continued to decrease over the E11.5-14.5 period (Fig. 4J) and into postnatal life (P1 and P28; data not shown). As seen at E9.5-10.5, only a few labeled cells were seen laterally, rostrally or radially away from the anterior DMT.

In contrast to the anterior DMT, posterior levels of the DMT – where the majority of tCPe cells reside – were devoid of Gdf7 cell lineages (Fig. 4B,C,E,F,K,L). The rostrocaudal level at which labeled tCPe and hem cells were no longer detectable approximated the level of the di-telencephalic midline boundary (Fig. 4). This suggested that anterior tCPe and hem cells are lineally related to Gdf7-expressing DM cells of neural tube stage embryos, while posterior tCPe and hem cells are not. The lack of posterior labeling was not due to mosaicism or inefficiency in R26R *lacZ* expression, as ACTBCre;R26R embryos demonstrated robust *lacZ* expression in apparently all tCPe and hem cells (data not shown). Likewise, Gdf7Cre mosaicism or insensitivity appears unlikely to account for the fate-mapping results, based on studies in ACTBCre;Gdf7DTA embryos (see below).

‘Late’ Gdf7-mediated ablation causes reduced mCPe and dCPe, but preserved tCPe

To confirm the genetic fate map, we mated Gdf7Cre to conditional Gdf7DTA (diphtheria toxin A chain) mice (Lee et al., 2000a; Monuki et al., 2001). In addition to optimal fidelity for Gdf7 cell lineages – both Cre and DTA should be restricted to Gdf7-expressing cells, thus minimizing transgene ‘leakiness’ – Gdf7Cre-mediated ablation should be delayed (‘late’) compared with ablations using ACTBCre mice. In ACTBCre;Gdf7DTA embryos, *Gdf7DTA* allele recombination should occur during very early embryogenesis (ACTBCre is expressed as early as the four-cell stage) (Lewandoski et al., 1997), resulting in ablation that coincides with the onset of Gdf7 expression. The same allele in Gdf7Cre;Gdf7DTA animals should not recombine until some time after Gdf7 expression onset, causing ablation to be relatively delayed. In contrast to the ACTBCre;Gdf7DTA phenotype (see below), Gdf7Cre;Gdf7DTA embryos were externally normal and viable through at least E16.5.

As predicted from the hindbrain and diencephalon fate maps (Fig. 3), late ablation resulted in reduced mCPe and dCPe. In E14.5 Gdf7Cre;Gdf7DTA embryos, mCPe reduction was grossly visible through the translucent hindbrain roof (data not

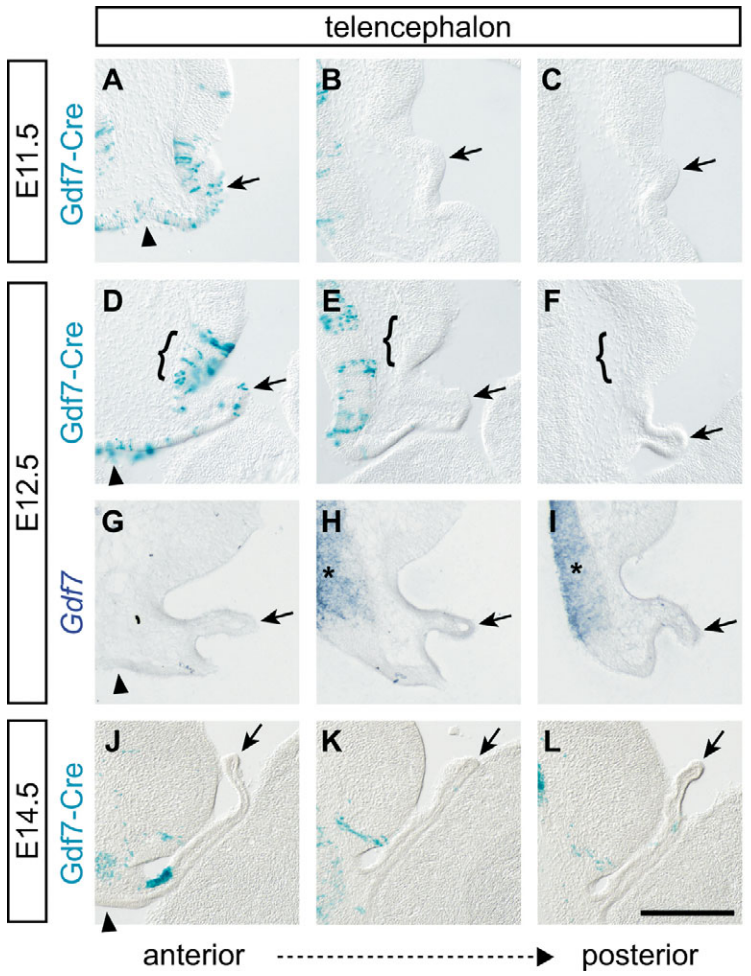

Fig. 4. Gdf7 cell lineages in the anterior, but not posterior, telencephalic CPe. X-gal stains (A-F,J-L) and Gdf7 in situ hybridization (G-I) on E11.5-14.5 Gdf7Cre;R26R or wild-type coronal cryosections. Semi-serial sections starting at the choroid plaque level are 120 μm (A-F,J-L) or 40-60 μm apart (G-I). Gdf7 cell lineages localize to the choroid plaque (arrowheads), tCPe (arrows) and cortical hem (brackets) in the anterior DMT (A,D,J). No tCPe or hem labeling is detected in the much-larger posterior DMT (B,C,E,F,K-L). In contrast to nearby diencephalic neuroepithelium (asterisks in H,I), Gdf7 mRNA is not detected in the tCPe or hem (arrows in G-I), which suggests true lineage relationships between the Gdf7-expressing DM cells at neural tube stages and the labeled anterior DMT cells at later stages. Scale bar: 0.2 mm.

shown). Ttr expression in the hindbrain and diencephalon was reduced at E12.5 (Fig. 5A,I) and E14.5 (Fig. 5C,K). Interestingly, Ttr expression remained detectable in both regions, particularly in the hindbrain. This raised the possibility that DTA-mediated ablation might still be ongoing at E14.5. As DTA causes cell death by inducing apoptosis (Komatsu et al., 1998), we used TUNEL assays to identify potential sites of ongoing DTA delivery. Significant apoptosis was present selectively in the residual dCPe and mCPe of E14.5 mutants (Fig. 5E,M), but not in control littermates or in other nearby tissues. By E16.5, papillary CP tissue was markedly reduced in both the hindbrain and diencephalon (Fig. 5G,O).

In contrast to the mCPe and dCPe, tCPe was well preserved in Gdf7Cre;Gdf7DTA embryos by histology (Fig. 6I), Ttr in situ hybridization (Fig. 6A,C), and TUNEL assays (Fig. 6E,G). Both anterior and posterior tCPe domains were maintained, although the volume of anterior tCPe appeared slightly reduced compared to normal (Fig. 6A). These tCPe findings correlated well with the Gdf7 fate map in the telencephalon (Fig. 4). The findings

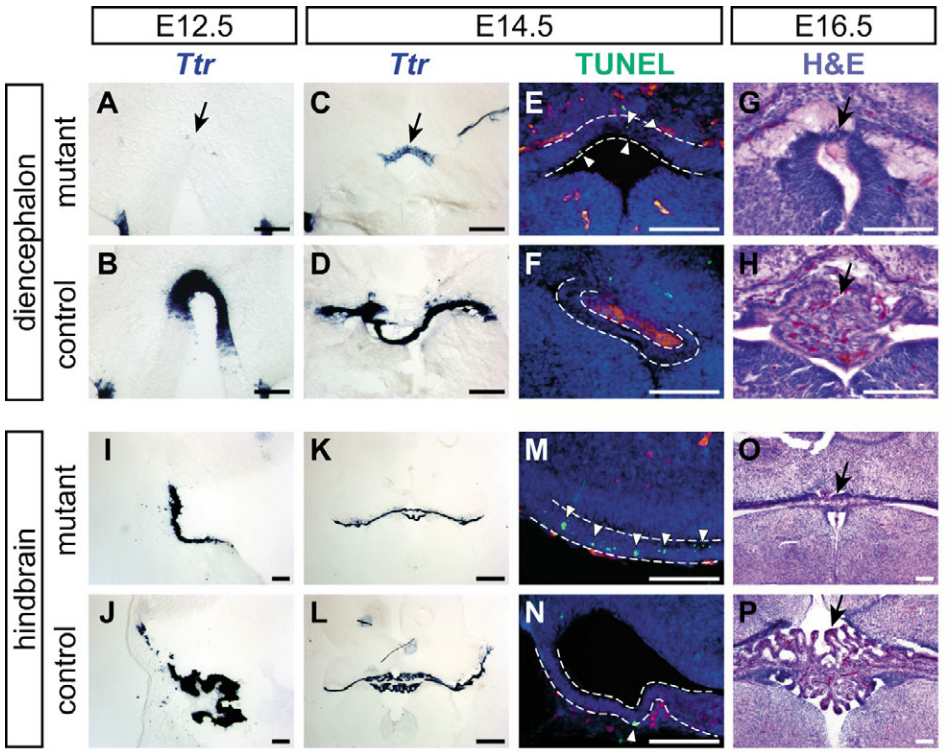

Fig. 5. Reduced diencephalic and myelencephalic CPe after late Gdf7-mediated ablation. Ttr in situ hybridization (A-D,I-L), fluorescent TUNEL assays (E,F,M,N; TUNEL green, nuclei blue, red blood cells yellow-orange), and Hematoxylin and Eosin (G,H,O,P; H&E) stains of E12.5-16.5 Gdf7Cre;Gdf7DTA coronal cryosections. (A-H) Diencephalon. The anterior diencephalic midline shows markedly reduced Ttr expression (A,C), increased apoptosis (E) and lack of papillary CP (G) in mutants compared with controls (B,D,F,H). (I-P) Hindbrain. As in the diencephalon, the mutant hindbrain shows reduced Ttr expression (I,K), increased apoptosis (M) and a lack of papillarity (O). Arrows designate CPe or its expected location; arrowheads designate TUNEL-positive cells; broken lines delimit the CPe. Scale bars: 0.4 mm in K,L; 0.1 mm in A-J,M-O.

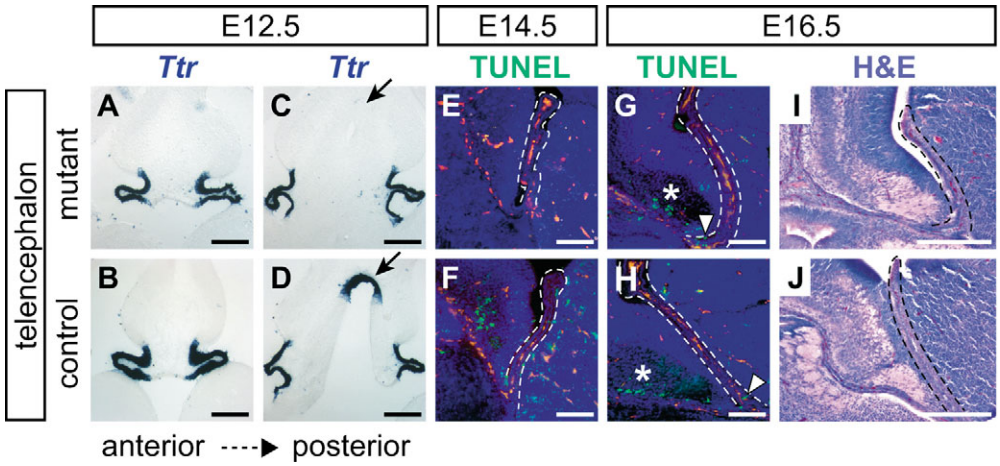

Fig. 6. Preserved telencephalic CPe after late Gdf7-mediated ablation. Ttr in situ hybridization (A-D), fluorescent TUNEL assays (E-H), and Hematoxylin and Eosin staining (I,J) as in Fig. 5. Anterior sections (A,B) at level of choroid plaque; posterior sections (C,D) at level of anterior diencephalon. Gdf7Cre;Gdf7DTA mutants maintain strong Ttr expression in the E12.5 telencephalon (A,C), in contrast to the diencephalon (arrow in C). Anterior tCPe volume appears slightly reduced (A) compared with normal (B). Significant tCPe apoptosis is not detected in mutant embryos (E,G), except at the CP base (arrowheads) and in the hippocampal mantle (asterisks), as seen in controls (H). The tCPe of E16.5 mutants appears normal histologically (I). Broken lines outline the CP. Scale bars: 0.2 mm.

at all CP sites suggested that CPe cells were ablated after their initial induction in Gdf7Cre;Gdf7DTA embryos.

The tCPe and dCPe emerge from separate developmental fields

The Gdf7 fate map and late ablation phenotype suggested significant differences between the tCPe and dCPe, but it was unclear whether they arise in continuous or separate developmental fields. In mice, papillary regions of dCPe and tCPe appear discontinuous, but are often separated by simple epithelium that resembles CPe (e.g. choroid plaque; Figs 4, 6). In humans and other species, the tCPe and dCPe appear continuous, but morphological studies have suggested that they form separately and then become continuous secondarily (Dziegielewska et al., 2001; Kappers, 1955).

To study the tCPe and dCPe fields in developing mice with a molecular marker, we examined Ttr expression in serial coronal sections. At E11.5, Ttr expression was detectable in the emerging tCPe bilaterally, but not yet in the diencephalon (Fig. 7A,B). Ttr expression became evident in dCPe by E12.5 (Fig. 7E,F), consistent with the conserved order of CP development in many species (i.e. tCP prior to dCP) (Dohrmann, 1970; Dziegielewska et al., 2001). In multiple embryos examined, Ttr expression was invariably separated into midline diencephalic and bilateral telencephalic fields by the Ttr-negative choroid plaque (Fig. 7A,D,E) and anterior diencephalic neuroepithelium (Fig. 7E,F). This indicated that the three forebrain CPe fields (two tCPe and one dCPe) are initially separate.

Apoptosis in 'early' Gdf7-mediated ablations coincides with the Gdf7 fate map

In order to ablate Gdf7-expressing cells at neural tube stages, we generated ACTBCre;Gdf7DTA embryos. In addition to synchronizing the ablation to Gdf7 expression onset, ACTBCre;Gdf7DTA embryos should be highly sensitive indicators of Gdf7 expression. Strong ACTBCre expression early in development (Lewandoski et al., 1997) results in little to no Cre mosaicism using this line (Meyers et al., 1998), which was confirmed in ACTBCre;R26R embryos (data not shown). In addition, as little as one DTA molecule can kill a cell (Yamaizumi et al., 1978), which makes cell death a sensitive readout of Gdf7 expression in ACTBCre;Gdf7DTA embryos.

As matings with ACTBCre mice on a mostly C57BL/6 background yielded confounding open forebrain defects (Monuki et al., 2001), we changed strain background in an attempt to correct the open forebrain phenotype. ACTBCre mice (Lewandoski et al., 1997) on an FVB/N background (Jackson Labs), when mated to the Gdf7DTA line, yielded

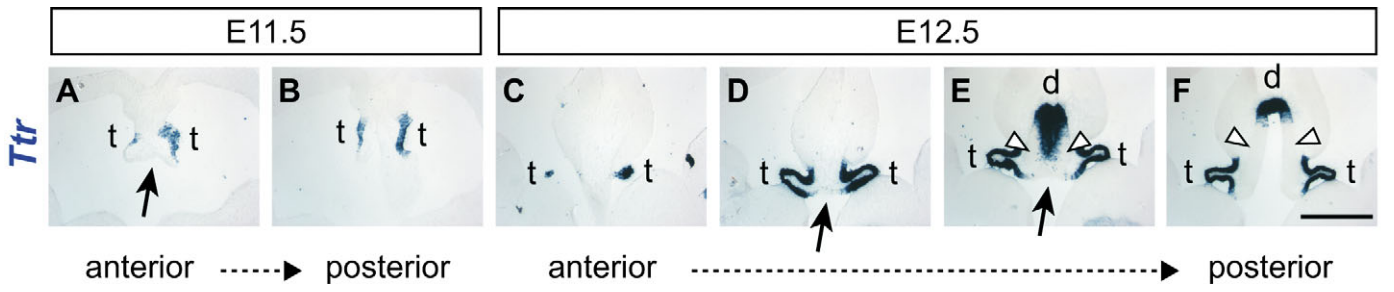

Fig. 7. Separation of the telencephalic and diencephalic CPe fields. Ttr in situ hybridization on E11.5-12.5 wild-type coronal cryosections. Semi-serial sections spanning the choroid plaque and anterior diencephalon are 40-80 μm apart. (A,B) E11.5 studies. Ttr-expressing tCPe domains are separated by the Ttr-negative choroid plaque (arrow in A). No diencephalic expression is detected at this stage. (C-F) E12.5 studies. Ttr expression commences in the dCPe, which is separated from the tCPe by Ttr-negative diencephalic neuroepithelium (arrowheads in E,F). Ttr-negative choroid plaque continues to separate the bilateral tCPe fields (arrows in D,E). d, dCPe; t, tCPe. Scale bar: 0.4 mm.

ACTBCre;Gdf7DTA embryos with closed forebrains in nearly 100% of cases (96/98 double transgenic embryos). Viable mutant embryos could be obtained through at least E14.5. More caudal CNS regions (including the hindbrain) remained open, as seen previously (Monuki et al., 2001), but the telencephalon and anterior diencephalon – where tCPe and dCPe form – were almost invariably closed.

Gross forebrain phenotypes in ACTBCre;Gdf7DTA embryos were evident by E10.5, suggesting that Gdf7-expressing DM cells were ablated at neural tube stages. To confirm this, we examined apoptosis by TUNEL assay in multiple E9.5-11.5 embryos. Apoptosis in the dorsal forebrain of E9.5 ACTBCre;Gdf7DTA embryos was restricted to the DM region, but elevated at anterior levels relative to controls (Fig. 8A). Apoptosis levels were at or below control levels by E10.0 (data not shown), E10.5 and E11.5 (Fig. 8G-R). These findings confirmed the predicted timing of DM cell ablation, as well as its apparent termination prior to definitive CPe differentiation.

At E10.5 and E11.5, apoptosis levels in the mutant telencephalon were low, but appreciable at the anterior midline (Fig. 8G,M), while significant TUNEL staining was absent at more posterior levels (Fig. 8H-I,N-O). This pattern was well matched to the apoptosis patterns seen in control littermates (Fig. 8J-L,P-R) and to the Gdf7 fate map (Fig. 4). These correspondences, together with the sensitivity of ACTBCre;Gdf7DTA embryos, confirm that the posterior tCPe domain lacks a significant cohort of Gdf7-expressing DM cell lineages. They also indicate that DM cell ablation at neural tube stages is the primary insult responsible for subsequent ACTBCre;Gdf7DTA phenotypes; we therefore refer to the ACTBCre;Gdf7DTA studies as 'DM cell ablations.'

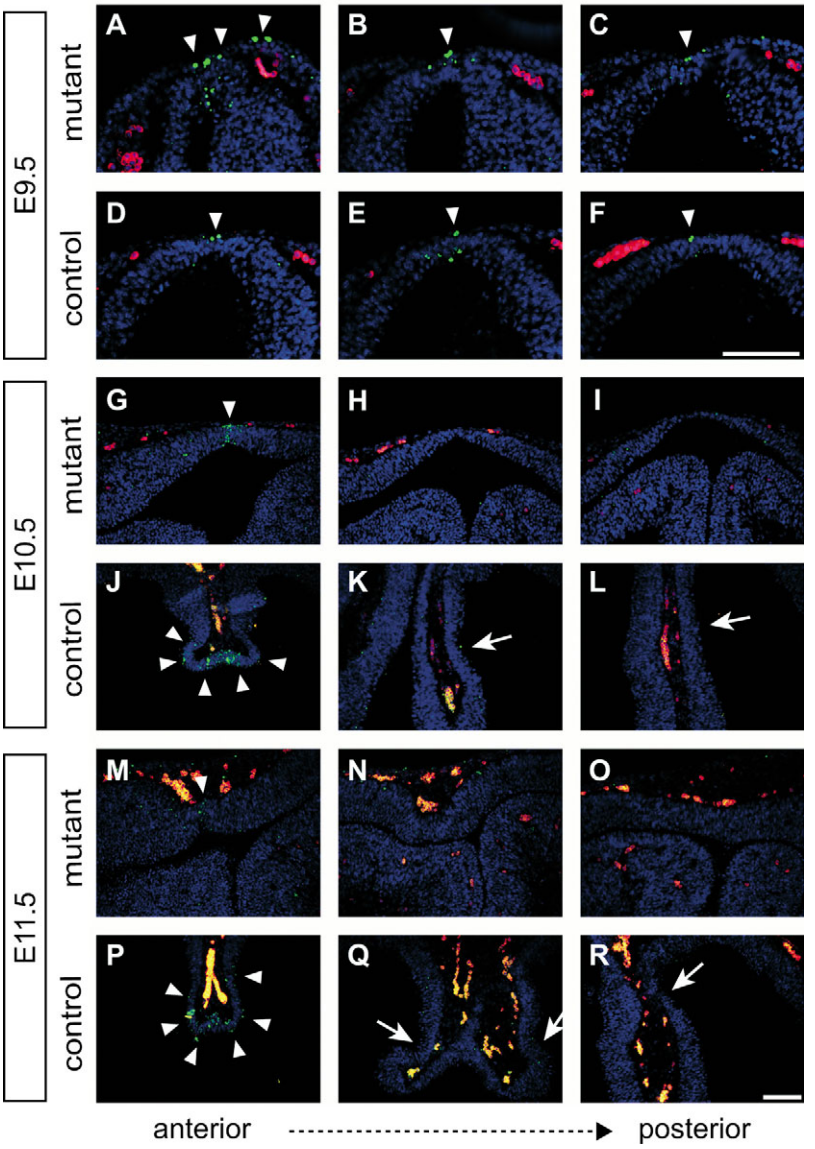

Fig. 8. DM apoptosis in normal embryos and after early Gdf7-mediated ablation. Fluorescent TUNEL assays (TUNEL, green; nuclei, blue; red blood cells, yellow-orange) on E9.5-11.5 ACTBCre;Gdf7DTA 10μm coronal cryosections. Semi-serial sections are 20-90 μm (A-F) or 120-250 μm (G-R) apart. (A-F) E9.5 studies. TUNEL labeling localizes to the midline region (neuroepithelium and overlying tissues) in mutants and controls. The increased labeling in mutants is consistent with enhanced apoptosis caused by DTA delivery. (G-L) E10.5 studies. Apoptosis in mutants is no longer elevated, but remains localized to the anterior midline, as seen in controls (G,J). In mutants, significant apoptosis is absent caudally where the posterior tCPe anlagen should reside (H,I). The normal posterior tCPe anlagen also displays negligible apoptosis (K,L). (M-R) E11.5 studies. Similar to the E10.5 findings, apoptosis is present at low levels in anterior midline of mutant embryos (M), while posterior levels show little to no apoptosis (N,O). In normal E11.5 embryos, the anterior tCPe demonstrates significant apoptosis (P), while the posterior tCPe does not (Q,R). Similar findings were seen in at least two embryos from each group/stage combination. Arrowheads designate TUNEL-positive regions; arrows designate the definitive tCPe or its anlagen. Scale bars: in F, 0.1 mm for A-F; in R, 0.1 mm for G-R.

Apoptosis in control embryos distinguishes the anterior and posterior tCPe domains

The anterior and posterior tCPe domains distinguished by Gdf7 fate mapping showed different patterns of apoptosis in normal embryos. At both E10.5 and E11.5, significant apoptosis was detectable in the choroid plaque and anterior tCPe (Fig. 8J,P), but not in the posterior tCPe domain (Fig. 8K-L,Q-R). As in the fate-mapping studies, the boundary between anterior and posterior tCPe domains detected by TUNEL was located lateral to, and at roughly the same rostrocaudal level as, the di-telencephalic midline boundary (Fig. 8).

DM cell ablation results in near-total tCPe loss

Unlike the late ablations, ACTBCre;Gdf7DTA embryos lacked tCPe almost entirely (Fig. 9). Neither histological evidence (Fig. 9E,G) nor Ttr expression (Fig. 9C) was detectable in most E12.5 mutants, although whole-mount in situ hybridization revealed minute Ttr domains in some embryos (data not

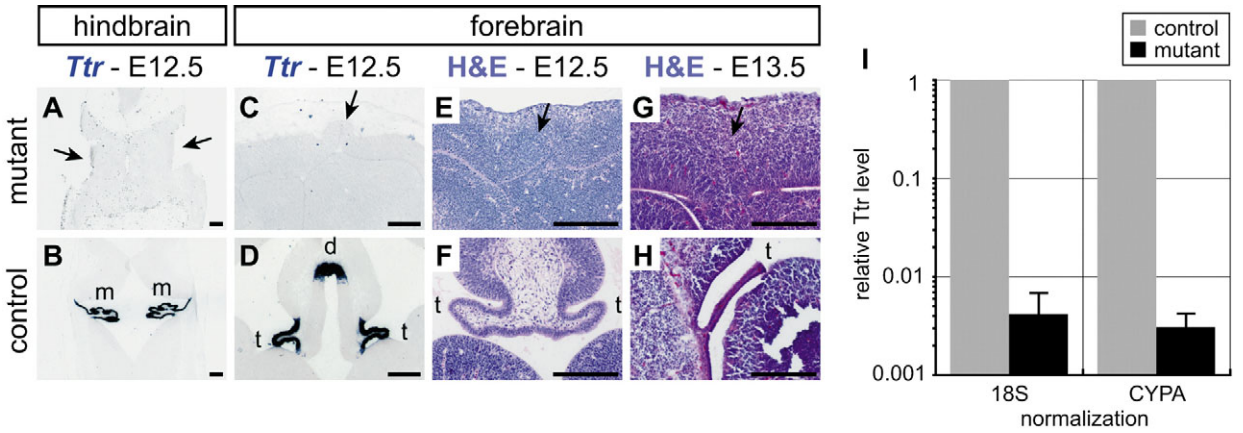

Fig. 9. Loss of all CPe, including posterior tCPe, after early Gdf7-mediated ablation. Ttr in situ hybridization and Hematoxylin and Eosin stains on E12.5 and E13.5 coronal cryosections (A-D,G,H) or paraffin sections (E,F), and Ttr qRT-PCR analysis (I) on E12.5 ACTBCre;Gdf7DTA embryos and controls. (A,B) Hindbrain. The mutant hindbrain is open and lacks Ttr expression (arrows in A). (C-I) Forebrain. In the closed mutant forebrain, no Ttr expression (C) or tissue resembling CP (F,H) is detectable at E12.5 (E) or E13.5 (G). (I) Ttr qRT-PCR. Ttr transcript levels in the dorsal forebrain are two to three orders of magnitude lower in the three E12.5 mutants relative to three littermate controls after normalizing to 18S rRNA (0.004±0.003) or Cyclophilin A (0.003±0.001). Arrows designate the expected sites of CPe; d, dCPe; m, mCPe; t, tCPe. Scale bars: 0.2 mm. See Materials and methods for additional qRT-PCR details.

shown). The apparent absence of tCPe was not due to developmental delay, as tCPe remained undetectable in E13.5 (Fig. 9G) and E14.5 mutants (data not shown).

To confirm the near-total tCPe loss, we developed a real-time semi-quantitative RT-PCR (qRT-PCR) assay for Ttr using stringent quality controls (Stankovic and Corfas, 2003) (see Materials and methods for details). When normalized to either of two internal reference genes, Ttr transcript levels were reduced by two to three orders of magnitude in the dorsal forebrains of three E12.5 ACTBCre;Gdf7DTA mutants compared with three littermate controls (Fig. 9I). Thus, Gdf7-expressing DM cells are required for posterior tCPe formation. As Gdf7 cell lineages do not contribute significantly to the posterior tCPe, the requirement for Gdf7-expressing DM cells is non-cell-autonomous. Furthermore, this DM cell requirement does not appear to involve a survival effect on posterior tCPe precursors, as the posterior telencephalon of ACTBCre;Gdf7DTA embryos lacked significant apoptosis (Fig. 8G-I,M-O).

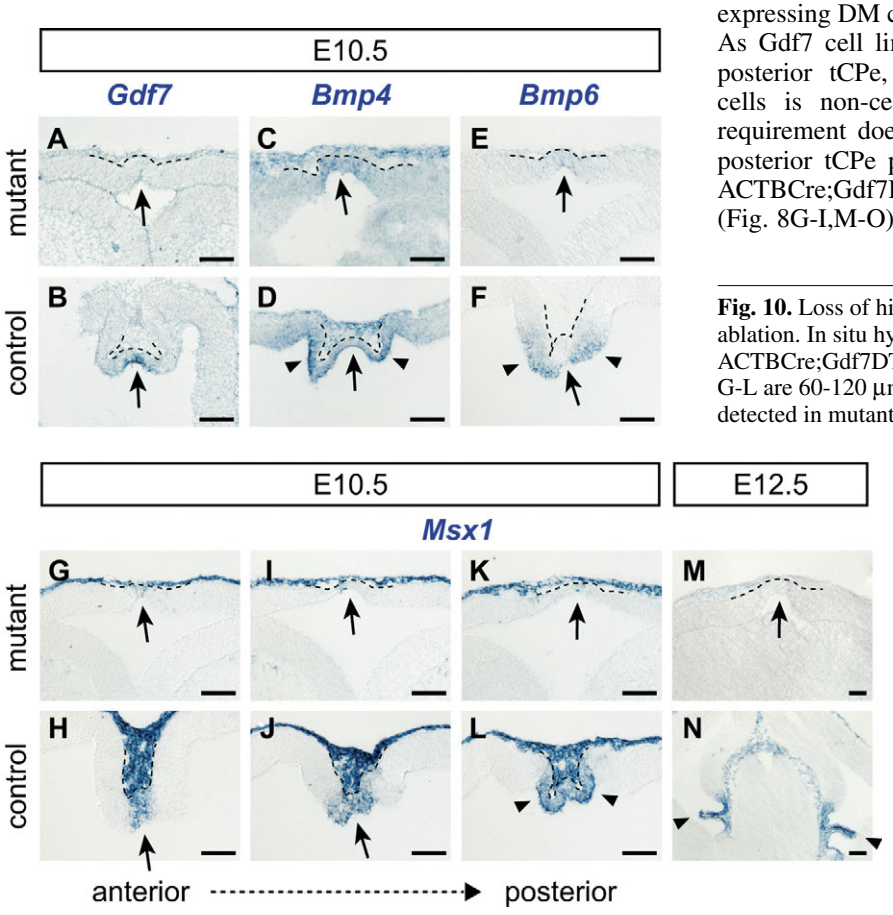

Fig. 10. Loss of high-level Bmp signaling after early Gdf7-mediated ablation. In situ hybridization on E10.5 and E12.5 ACTBCre;Gdf7DTA coronal cryosections. Semi-serial sections in G-L are 60-120 μm apart. (A-F) Bmp studies. Gdf7 is no longer detected in mutants (A), consistent with ablation. In controls, Bmp4 (D) and Bmp6 levels (F) are higher in the bilateral tCPe anlagen (arrowheads) and lower at the midline (arrows). After ablation, Bmp4 and Bmp6 levels are reduced and confined to a small midline domain (C,E). Epidermal/mesenchymal Bmp4 expression is maintained after ablation (C). (G-N) Msx1 studies. Msx1 is expressed in the tCPe anlagen at E10.5 (L) and in the definitive tCPe at E12.5 (N). After ablation, Msx1 expression in the neuroepithelium is dramatically reduced at E10.5 (G,I,K) and E12.5 (M). In situ hybridization of sections adjacent to those in A and M demonstrate well-preserved mRNA. Broken lines outline the neuroepithelium; arrows indicate the midline; arrowheads indicate tCPe or its anlagen. Scale bars: 0.1 mm.

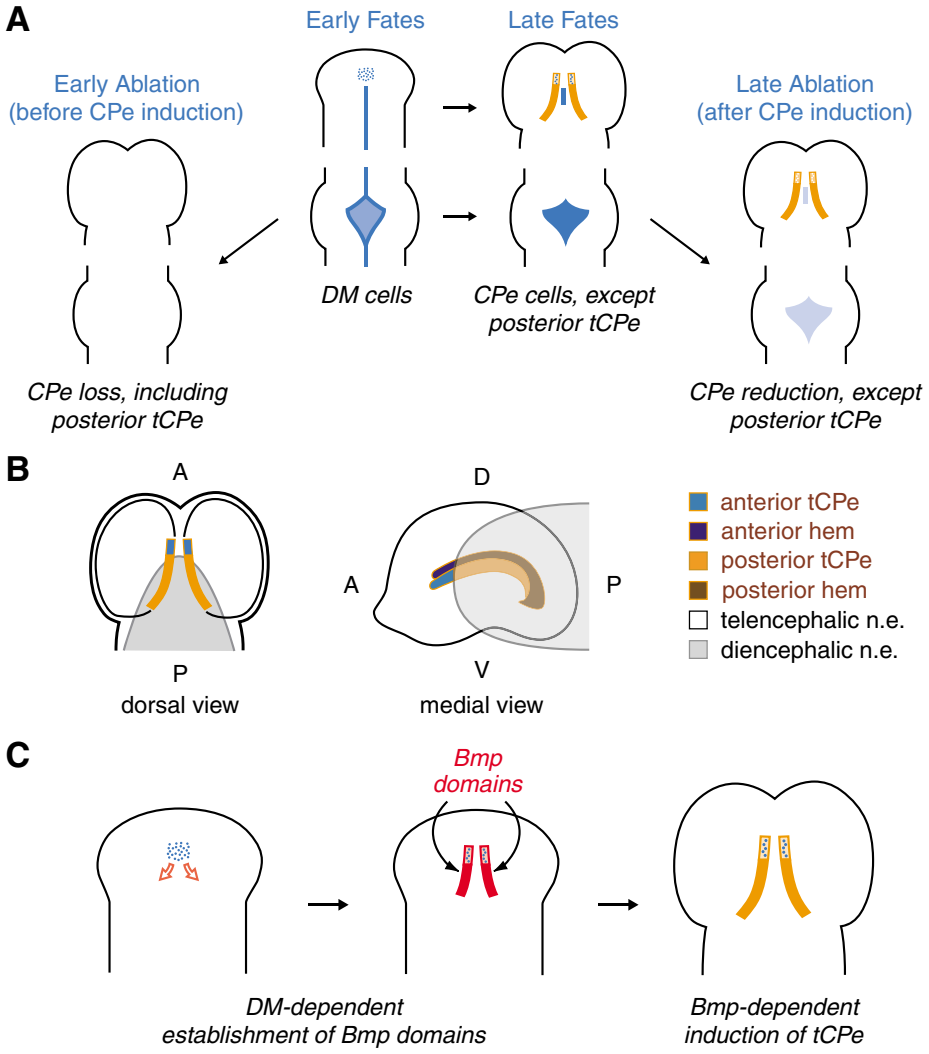

Fig. 11. DM-CPe relationships. (A) Summary of the Gdf7 fate map and ablation studies; color-coding as in Fig. 1, with blue denoting DM or CPe domains with apparent lineage relationships to DM cells. Many mCPe and dCPe cells are derived directly from DM cells. In the telencephalon, DM cell lineages contribute to the anterior tCPe domain, but not to the posterior tCPe (orange). Late Gdf7-mediated ablation results in mCPe and dCPe reduction, but preserved posterior tCPe, consistent with ablation after CPe induction. By contrast, early ablation of Gdf7-expressing DM cells causes near total loss of CPe, including the posterior tCPe. (B) The distinct anterior and posterior tCPe domains; dorsal and medial views, as in Fig. 1. The anterior domain contains DM cell lineages and exhibits marked apoptosis, while the larger posterior domain lacks these features. The two domains are separated by a cryptic boundary located lateral to the di-telencephalic midline boundary. A similar domain structure applies to the adjacent cortical hem. (C) Model of DM-dependent tCPe induction. DM cells are required to establish high-level Bmp signaling in the tCPe anlagen (red). In the anterior domain, both cell-autonomous and non-cell-autonomous mechanisms are involved, whereas posterior domain establishment is non-autonomous. In both domains, homeogenetic mechanisms may be involved (see Discussion for details). Following its establishment, high-level Bmp signaling is then responsible for locally inducing the tCPe (orange) (Hebert et al., 2002).

DM cell ablation causes reduced Bmp expression and signaling

As local high-level Bmp signaling has been implicated in tCPe induction (Hebert et al., 2002), we asked whether deficient Bmp signaling could account for the tCPe loss in ACTBCre;Gdf7DTA embryos. As described previously (Furuta et al., 1997), Bmp6 was selectively expressed in the DM neuroepithelium, while Bmp4 and Bmp7 had additional expression domains in overlying non-neural tissues of normal E10.5 embryos (Fig. 10D,F; data not shown). Gdf7 (Bmp12) expression was detectable in the midline (Fig. 10B), while Bmp4 and Bmp6 levels were lower at the midline and higher in bilateral domains corresponding to the tCPe anlagen (Fig. 10D,F).

In addition to the expected loss of Gdf7 (Fig. 10A), the three other Bmps were reduced in level, as well as extent, in the DM neuroepithelium of E10.5 ACTBCre;Gdf7DTA embryos (Fig. 10C,E; data not shown). Residual Bmp4, Bmp6 and Bmp7 expression in mutants persisted in a small midline field, in contrast to the bilaterally paired domains seen normally (Fig. 10D,F). The persistent low-level Bmp expression was consistent with the ablation of some, but not all, DM cells, as predicted from the Gdf7 fate map (Fig. 4).

To determine whether the reduced Bmp levels led to reduced Bmp signaling, we examined Msx1 expression, a standard marker of high-level Bmp signaling in the developing forebrain (Furuta et al., 1997; Hebert et al., 2002; Shimamura and Rubenstein, 1997). In normal embryos, Msx1 expression correlated well with sites of high-level Bmp expression, including the bilateral tCPe anlagen at E10.5 (Fig. 10L) and the definitive tCPe at E12.5 (Fig. 10N). In E10.5 and E12.5 ACTBCre;Gdf7DTA embryos, neuroepithelial Msx1 expression was almost completely absent, while expression persisted in the attenuated non-neural tissues overlying the neuroepithelium (Fig. 10G,I,K,M). Thus, high-level neuroepithelial Bmp signaling was almost completely abrogated after DM cell ablation.

Discussion

Our studies provide evidence for essential DM-CPe relationships at all sites of CP formation (Fig. 11A). CPe cells of the hindbrain, diencephalon and anterior tCPe domain appear to include the descendants of Gdf7-expressing DM cells. By contrast, the posterior tCPe domain lacks these descendants, but requires DM cells in a non-cell-autonomous

fashion for its genesis. In addition to the lineage differences, apoptosis distinguishes the anterior and posterior tCPe domains, which are separated by a boundary located at approximately the same rostrocaudal level as the di-telencephalic midline boundary (Fig. 11B). The tCPe loss caused by DM cell ablation is preceded by a failure to generate high-level Bmp signaling, which presages the tCPe (Fig. 10D,F,L) and induces its formation (Hebert et al., 2002). This failure, coupled with the lack of a simple survival effect, suggests that DM cells induce high-level Bmp signaling, which in turn induces the posterior tCPe (Fig. 11C).

DM-CPe relationships in the hindbrain and diencephalon

Classical morphological studies have long suggested that the RP invaginates and directly becomes mCPe and dCPe (Dohrmann, 1970). A more recent study, which employed intersectional fate mapping with Wnt1 and Hoxa2-driven Cre and Flp lines, also concluded that the hindbrain RP and mCPe are derived from the same embryonic primordium (Awatramani et al., 2003). Our studies are consistent with these conclusions; however, it should be noted again that our fate-mapping data in the hindbrain and diencephalon are not conclusive with regard to lineage. As discussed earlier, Gdf7-expressing mCPe and dCPe cells could be derived from Gdf7-negative precursors, although it seems highly unlikely that such lineages account for all of the mCPe and dCPe.

DM cell lineages in the telencephalon

In the telencephalon, the lack of Gdf7 transcripts after E10.5 (Fig. 4G-I) makes lineage assignment based on the genetic fate map more definitive. Based on this map, Gdf7 cell lineages at E11.5-12.5 are primarily found in the choroid plaque, tCPe and cortical hem of the anterior DMT. We have previously shown that Gdf7 lineages also include cortical marginal zone (MZ) neurons that appear to originate from the cortical hem (Monuki et al., 2001). The hem is a significant source of MZ neurons (Meyer et al., 2002; Takiguchi-Hayashi et al., 2004), but our current study indicates that only a small fraction of hem cells and their MZ progeny belong to Gdf7 lineages.

Three different genetic strategies (Gdf7Cre;R26R, Gdf7Cre;Gdf7DTA, ACTBCre;Gdf7DTA) provided evidence that Gdf7 cell lineages do not contribute significantly to the posterior DMT. Cre mosaicism or insensitivity seems insufficient to account for these findings for at least two reasons. First, Gdf7 fate mapping with Gdf7Cre;R26R embryos was more sensitive than Gdf7 in situ hybridization in the telencephalon (compare Fig. 2, Fig. 4 and Fig. 10B). Second, as discussed earlier, the ACTBCre;Gdf7DTA studies were highly unlikely to suffer from significant mosaicism or insensitivity. Indeed, ACTBCre;Gdf7DTA embryos should be among the least mosaic and most sensitive Gdf7 expression indicators possible using mouse genetics. Thus, the absence of significant apoptosis away from the anterior midline of ACTBCre;Gdf7DTA embryos (Fig. 8) makes it highly unlikely that Gdf7 cell lineages constitute a significant fraction of the posterior DMT.

The anterior and posterior domains of tCPe

The tCPe domains distinguished by Gdf7 fate mapping (Fig. 4) and apoptosis (Fig. 8) are separated by a boundary that is not apparent morphologically (Fig. 11B). This ‘cryptic’ tCPe boundary appears to be analogous to those described recently in the hindbrain DM and CPe (Awatramani et al., 2003); such cryptic boundaries may therefore be general features of the DM and CPe. The Gdf7 cell lineages themselves may undergo apoptosis in the anterior tCPe. These lineages constitute a decreasing fraction of anterior tCPe and other DMT cells over time (Fig. 4; data not shown), suggesting higher apoptosis:proliferation ratios in Gdf7 cell lineages compared with their neighbors. These lineages also cluster towards the base of tCPe at later stages (e.g. Fig. 4J), where apoptosis may be selectively seen (Fig. 6G,H).

Interestingly, anterior and posterior domains within human tCPe, with features remarkably similar to those described in our study, have been described in a classic monograph (Bailey, 1915). In this neuroanatomical study of human embryos, Bailey concluded that the anterior tCPe is derived directly from the paraphyseal arch, the region of telencephalic RP just anterior to the transverse fold (velum transversum) that demarcates the boundary between telencephalic and diencephalic RP. Anterior tCPe is continuous with and lateral to the paraphyseal arch, where it forms in the ‘area choroidea anterior.’ Temporally, anterior tCPe differentiation occurs slightly ahead of the posterior tCPe, which is much more voluminous and forms in the ‘area choroidea posterior’ along the medial telencephalic wall. Our study fully supports these conclusions, including the direct derivation of anterior tCPe cells from the RP (DM), the separate derivation of posterior tCPe from the medial telencephalic wall, and the anteroposterior tCPe boundary being located lateral to, and at a similar rostrocaudal level as, the velum transversum (di-telencephalic midline boundary). The similarities between our mouse studies and the Bailey monograph on human embryos suggest a common tCPe substructure that is likely to be shared among mammals.

The non-cell-autonomous DM-tCPe relationship

Our studies suggest a model in which DM cells act non-cell-autonomously to generate high-level Bmp signaling in the posterior tCPe anlagen, which subsequently leads to CPe induction (Hebert et al., 2002) (Fig. 11C). Lower-level Bmp signaling, as seen in the normal choroid plaque (Figs 7, 10) and in the midline after DM cell ablation (Figs 9, 10), is insufficient to induce CPe. As DM cells have no apparent influence on cell survival in the posterior tCPe domain (Fig. 8), the DM cells are likely to generate high-level Bmp signaling via an active inductive process. The critical period for this non-cell-autonomous process includes E9.0-9.5, based on the timing of DM cell ablation in ACTBCre;Gdf7DTA embryos (Fig. 8); ablation in Gdf7Cre;Gdf7DTA embryos occurs after the inductive period (Fig. 6). E9.0-9.5 would overlap the permissive period for inducing CPe in mouse forebrain cells (E8.5-9.5) (Thomas and Dziadek, 1993).

The likelihood that DM cells not only become tCPe cells, but also induce them non-cell-autonomously, implies that homeogenetic mechanisms are involved in tCPe induction. Homeogenetic induction – i.e. the ability of a cell to induce its neighbor to adopt a fate similar to its own – is a well known feature of the ventral (Placzek et al., 1993) and dorsal (Liem et al., 1995) midlines in the developing spinal region, and has been described for Gdf7-expressing RP cells near the isthmus

organizer (Alexandre and Wassef, 2003). In addition to inducing posterior tCPe cells, homeogenetic mechanisms may be involved in the anterior domain, where tCPe cells derived from Gdf7-negative precursors also fail to form after Gdf7-mediated ablation. Bmps mediate homeogenesis in the dorsal spinal cord (Liem et al., 1997; Liem et al., 1995) and may be the crucial homeogenetic signals in tCPe induction (Fig. 10, Fig. 11C). Indeed, the residual midline domains of Bmp4 and Bmp6 following DM cell ablation (Fig. 10C,E) would be consistent with a failure of Bmp production to spread homeogenetically from the DM into the tCPe anlagen.

We thank Kevin Lee and Tom Jessell for the Gdf7 mice; Anne Calof, Candice Crocker, and Julie Lauterborn for in situ hybridization templates; Chris Walsh for his support of the Gdf7 project; and Lisa Flanagan, Karla Hirokawa, Georg Streidter, and anonymous reviewers for comments on this manuscript. This work was supported by an NIH K08 award, the March of Dimes Birth Defects Foundation, the Whitehall Foundation, and the UCI Department of Pathology (ESM).

References

Alexandre, P. and Wassef, M. (2003). The isthmic organizer links anteroposterior and dorsoventral patterning in the mid/hindbrain by generating roof plate structures. *Development* **130**, 5331-5338.

Awatramani, R., Soriano, P., Rodriguez, C., Mai, J. J. and Dymecki, S. M. (2003). Cryptic boundaries in roof plate and choroid plexus identified by intersectional gene activation. *Nat. Genet.* **35**, 70-75.

Bailey, P. (1915). Morphology of the roof plate of the forebrain and the lateral choroid plexuses in the human embryo. *J. Comp. Neurol.* **26**, 79-120.

Chizhikov, V. V. and Millen, K. J. (2005). Roof plate-dependent patterning of the vertebrate dorsal central nervous system. *Dev. Biol.* **277**, 287-295.

Dohrmann, G. J. (1970). The choroid plexus: a historical review. *Brain Res.* **18**, 197-218.

Dziegielewska, K. M., Ek, J., Habgood, M. D. and Saunders, N. R. (2001). Development of the choroid plexus. *Microsc. Res. Tech.* **52**, 5-20.

Furuta, Y., Piston, D. W. and Hogan, B. L. (1997). Bone morphogenetic proteins (BMPs) as regulators of dorsal forebrain development. *Development* **124**, 2203-2212.

Grove, E. A., Tole, S., Limon, J., Yip, L. and Ragsdale, C. W. (1998). The hem of the embryonic cerebral cortex is defined by the expression of multiple Wnt genes and is compromised in Gli3-deficient mice. *Development* **125**, 2315-2325.

Harms, P. J., Tu, G. F., Richardson, S. J., Aldred, A. R., Jaworowski, A. and Schreiber, G. (1991). Transthyretin (prealbumin) gene expression in choroid plexus is strongly conserved during evolution of vertebrates. *Comp. Biochem. Physiol. B* **99**, 239-249.

Hebert, J. M., Mishina, Y. and McConnell, S. K. (2002). BMP signaling is required locally to pattern the dorsal telencephalic midline. *Neuron* **35**, 1029-1041.

Herbert, J., Wilcox, J. N., Pham, K. T., Fremeau, R. T., Jr, Zeviani, M., Dwork, A., Soprano, D. R., Makover, A., Goodman, D. S., Zimmerman, E. A. et al. (1986). Transthyretin: a choroid plexus-specific transport protein in human brain. The 1986 S. Weir Mitchell award. *Neurology* **36**, 900-911.

Kappers, J. A. (1955). The development of the paraphysis cerebri in man with comments on its relationship to the intercolumnar tubercle and its significance for the origin of cystic tumors in the third ventricle. *J. Comp. Neurol.* **102**, 425-509.

Kaufman, M. H. and Bard, J. B. L. (1999). *The Anatomical Basis of Mouse Development.* San Diego, CA: Academic Press.

Komatsu, N., Oda, T. and Muramatsu, T. (1998). Involvement of both caspase-like proteases and serine proteases in apoptotic cell death induced by ricin, modeccin, diphtheria toxin, and pseudomonas toxin. *J. Biochem. (Tokyo)* **124**, 1038-1044.

Lee, K. J., Dietrich, P. and Jessell, T. M. (2000a). Genetic ablation reveals that the roof plate is essential for dorsal interneuron specification. *Nature* **403**, 734-740.

Lee, S. M., Tole, S., Grove, E. and McMahon, A. P. (2000b). A local Wnt-3a signal is required for development of the mammalian hippocampus. *Development* **127**, 457-467.

Lewandoski, M., Meyers, E. N. and Martin, G. R. (1997). Analysis of *Fgf8* gene function in vertebrate development. *Cold Spring Harbor Symp. Quant. Biol.* **62**, 159-168.

Liem, K. F., Jr, Tremml, G., Roelink, H. and Jessell, T. M. (1995). Dorsal differentiation of neural plate cells induced by BMP-mediated signals from epidermal ectoderm. *Cell* **82**, 969-679.

Liem, K. F., Jr, Tremml, G. and Jessell, T. M. (1997). A role for the roof plate and its resident TGFbeta-related proteins in neuronal patterning in the dorsal spinal cord. *Cell* **91**, 127-138.

Livak, K. J. and Schmittgen, T. D. (2001). Analysis of relative gene expression data using real-time quantitative PCR and the 2(–Delta Delta C(T)) Method. *Methods* **25**, 402-408.

Meyer, G., Perez-Garcia, C. G., Abraham, H. and Caput, D. (2002). Expression of p73 and Reelin in the developing human cortex. *J. Neurosci.* **22**, 4973-4986.

Meyers, E. N., Lewandoski, M. and Martin, G. R. (1998). An Fgf8 mutant allelic series generated by Cre- and Flp-mediated recombination. *Nat. Genet.* **18**, 136-141.

Millonig, J. H., Millen, K. J. and Hatten, M. E. (2000). The mouse Dreher gene *Lmx1a* controls formation of the roof plate in the vertebrate CNS. *Nature* **403**, 764-769.

Monuki, E. S., Porter, F. D. and Walsh, C. A. (2001). Patterning of the dorsal telencephalon and cerebral cortex by a roof plate-Lhx2 pathway. *Neuron* **32**, 591-604.

Placzek, M., Jessell, T. M. and Dodd, J. (1993). Induction of floor plate differentiation by contact-dependent, homeogenetic signals. *Development* **117**, 205-218.

Shimamura, K. and Rubenstein, J. L. (1997). Inductive interactions direct early regionalization of the mouse forebrain. *Development* **124**, 2709-2718.

Soriano, P. (1999). Generalized lacZ expression with the ROSA26 Cre reporter strain. *Nat. Genet.* **21**, 70-71.

Stankovic, K. M. and Corfas, G. (2003). Real-time quantitative RT-PCR for low-abundance transcripts in the inner ear: analysis of neurotrophic factor expression. *Hear. Res.* **185**, 97-108.

Sturrock, R. R. (1979). A morphological study of the development of the mouse choroid plexus. *J. Anat.* **129**, 777-793.

Takiguchi-Hayashi, K., Sekiguchi, M., Ashigaki, S., Takamatsu, M., Hasegawa, H., Suzuki-Migishima, R., Yokoyama, M., Nakanishi, S. and Tanabe, Y. (2004). Generation of reelin-positive marginal zone cells from the caudomedial wall of telencephalic vesicles. *J. Neurosci.* **24**, 2286-2295.

Thomas, T. and Dziadek, M. (1993). Capacity to form choroid plexus-like cells in vitro is restricted to specific regions of the mouse neural ectoderm. *Development* **117**, 253-262.

Wang, X. and Seed, B. (2003). A PCR primer bank for quantitative gene expression analysis. *Nucleic Acids Res.* **31**, e154.

Wilting, J. and Christ, B. (1989). An experimental and ultrastructural study on the development of the avian choroid plexus. *Cell Tissue Res.* **255**, 487-494.

Yamaizumi, M., Mekada, E., Uchida, T. and Okada, Y. (1978). One molecule of diphtheria toxin fragment A introduced into a cell can kill the cell. *Cell* **15**, 245-250.

Yamamoto, M., McCaffery, P. and Drager, U. C. (1996). Influence of the choroid plexus on cerebellar development: analysis of retinoic acid synthesis. *Dev. Brain Res.* **93**, 182-190.